



An insider view of the Portuguese ion beam laboratory

E. Alves^{1,a}, K. Lorenz^{1,2,b} , N. Catarino¹, M. Peres¹, M. Dias¹, R. Mateus¹,
L. C. Alves³, V. Corregidor^{3,c} , N. P. Barradas³, M. Fonseca⁴, J. Cruz⁴, A. Jesus⁴

¹ IPFN, Instituto Superior Técnico, Universidade de Lisboa, Campus Tecnológico e Nuclear, Estrada Nacional N° 10, km 139.7, 2695-066 Bobadela, Portugal

² INESC MN, Rua Alves Redol 9, 1000-029 Lisboa, Portugal

³ C2TN, Instituto Superior Técnico, Universidade de Lisboa, Campus Tecnológico e Nuclear, Estrada Nacional N° 10, km 139.7, 2695-066 Bobadela, Portugal

⁴ Laboratório de Instrumentação, Engenharia Biomédica e Física da Radiação (LIBPhys-UNL), Departamento de Física, Faculdade de Ciências e Tecnologia, Universidade Nova de Lisboa, Monte da Caparica, 2892-516 Caparica, Portugal

Received: 22 December 2020 / Accepted: 31 May 2021

© The Author(s), under exclusive licence to Società Italiana di Fisica and Springer-Verlag GmbH Germany, part of Springer Nature 2021

Abstract Accelerators are behind many major scientific and technological breakthroughs giving a gigantic contribution to unveil the mysteries of matter. This quest continues nowadays using the high-energy machines operating at large research centres like CERN, GANIL and FAIR, among others. Meanwhile most of the small and medium size accelerators running in laboratories located in universities and research institutions around the world begin a new life making available the powerful nuclear-based techniques for multidisciplinary research in several domains. Furthermore, the small and medium size accelerator facilities still play a major role in keeping and providing knowledge in Nuclear Science and training the new generations. The two electrostatic accelerators at Instituto Superior Técnico of the University of Lisbon are devoted to multidisciplinary research as well as education and training students in nuclear-based experimental techniques. The history and work carried out in the laboratory and its role in areas with great societal impact such as materials science, energy, biomedical sciences as well as nuclear experimental physics in support of the large-scale facilities, will be highlighted in the manuscript.

1 Introduction

Since the early thirties of the twentieth century, when the first operational electrostatic accelerators became available to the scientific community, a long road was walked until the present days where TeV machines are used at CERN. In 1932, Van de Graaff developed the belt-charged generator accelerator and the first applications in nuclear physics were the base for a tremendous boom observed in the experimental work in the field. The possibility to choose the energy, intensity and mass of the beam particles offered the opportunity to look into

^a e-mail: ealves@ctn.tecnico.ulisboa.pt (corresponding author)

^b e-mail: lorenz@ctn.tecnico.ulisboa.pt (corresponding author)

^c e-mail: vicky.corregidor@ctn.tecnico.ulisboa.pt

the nucleus and created a great enthusiasm in the scientific community. In the fifties of last century, the Portuguese government decided to build a nuclear campus for research with a nuclear research reactor and a laboratory then equipped with a 2.0 MV Van de Graaff and a 600 kV Cockroft–Walton accelerator. Inaugurated in January 1961, these were the early days of the actual Laboratory of Accelerators and Radiation Technologies (LATR) of Instituto Superior Técnico (IST), the engineering school of the University of Lisbon. Since then, the laboratory has undergone several transformations with new machines installed and several upgrades, leading the infrastructure to a consolidated position, internationally recognised for the quality of the work performed by LATR researchers and collaborators.

LATR is a research and development laboratory of IST with a deputy-director appointed by the President of IST. The salaries of the staff, technicians and researchers, as well as the running costs are covered by the university budget. The research staff is responsible for the operation of the experimental lines making ion beam-based techniques available to the scientific community in the country and abroad. The collaboration with research groups from other institutions is encouraged in order to apply for financing through research projects funded by national and international agencies (EU mostly). This funding is very important to keep the equipment at state-of-the-art condition and install new upgrades. Besides the close interactions with the scientific community in the country, the laboratory is well acknowledged internationally and participated in some relevant projects during the last decades.

In addition to financial support, technical and scientific expert assistance and collaboration in TC and CRP projects promoted by IAEA since the early beginnings of the nuclear campus, LATR was partner in the FP7 project SPIRIT (2009–2013): *Support of Public and Industrial Research Using Ion Beam Technology (GA 227012CPCSAInfra)*, where 11 ion beam facilities in Europe gathered to offer transnational access to external users. In 2013–2017 the same consortium of laboratories ran a Marie Curie action, *SPRITE-Supporting Postgraduate Research with Internships in industry and Training Excellence (FP7-PEOPLE-2012-ITN, Grant agreement no. 317169)* to spread the ion beam technologies around the world. Several Early Stage Researchers (ESR) were trained within this network. Currently, the laboratory is member of the RADIATE project: *Research and Development with Ion Beams—Advancing Technology in Europe (H2020-INFRAIA-2018–1)* with 18 partners.

Moreover, there has been a continuous participation on the European Fusion programme (EFDA), now EUROfusion, since 1998 using the ion beam techniques to study materials and plasma wall interactions in fusion devices. The erosion/redeposition processes and fuel retention have been studied in detail and will be highlighted in Sect. 3.1a. Some of the activities related to fusion science were also covered under the umbrella of several International Atomic Energy Agency (IAEA) Coordinated Research Projects and we are now working on the projects: *Development and Application of Ion Beam Techniques for Materials Irradiation and Characterisation relevant to Fusion Technology* and *Pathways to Energy from Inertial Fusion: Materials Research and Technology*.

Furthermore, many national and international projects funded in competitive calls were developed in the areas of Functional Materials (cf. Sect. 3.1b), Cultural Heritage (cf. Sect. 3.1c), biomedical applications, Nuclear Reactions (cf. Sect. 3.2), among others. The importance of all these activities is well documented in the long list of publications in journals of reference some of them included in this work. Some examples of the more relevant outcomes will be discussed in the following paragraphs.

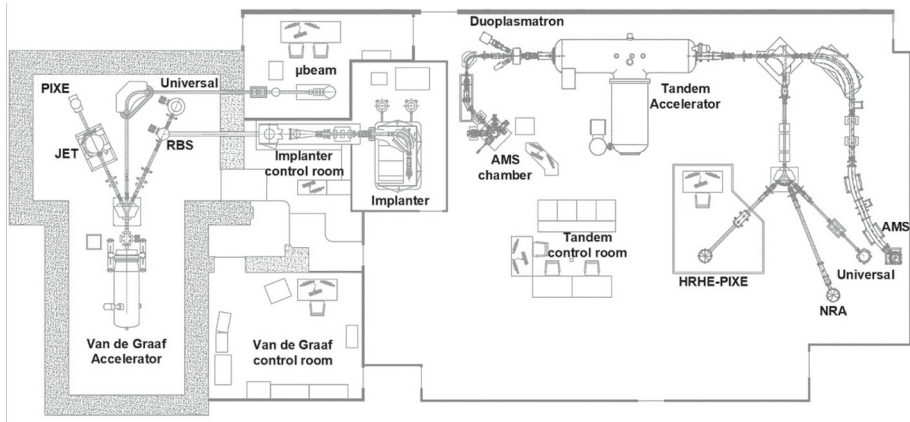


Fig. 1 Portrait of the accelerators room of the Laboratory of Accelerators and Radiation Technologies (LATR)

2 Experimental and technical details

The Laboratory of Accelerators and Radiation Technologies is an infrastructure hosting two electrostatic accelerators, an ion implanter, an ion microprobe with both in-vacuum and external beam setups, two high-resolution X-ray diffractometers, a micro-AMS (accelerator mass spectrometry) system and a high-resolution high-energy (HRHE) particle-induced X-ray emission (PIXE) setup, Fig. 1.

A 2.5 MV Van de Graaff accelerator was installed in 1991 and is equipped with three experimental beam lines including an ion microprobe. One line is equipped with two multipurpose Ion Beam Analysis (IBA) chambers, one with a high-resolution Rutherford Backscattering Spectrometry (RBS) system and an elastic recoil detection (ERDA) setup for hydrogen isotope detection. Another experimental line with a dedicated IBA chamber is equipped to handle large and contaminated samples (European Fusion Programme) and a PIXE chamber (Fig. 2).

The nuclear microprobe was installed in 1999 [1] and in 2008 the external-ion microbeam analytical end-station became operational, adding a set of valuable analytical techniques for the community involved in the study and conservation of Cultural Heritage in Portugal and abroad, Fig. 3. Based on the OM150 system from Oxford Microbeams, the in-vacuum setup allows focusing the beam down to $3 \times 4 \mu\text{m}^2$ for routine analysis when using high current IBA techniques (as PIXE and RBS) or attain sub-micrometer spatial resolution when using low current IBA techniques (such as on-axis Scanning Transmission Ion Microscopy (STIM) or Ion Beam Induce Charge (IBIC)) with the possibility of scanning the beam in a sample area of $2640 \times 2640 \mu\text{m}^2$ (for 2 MeV protons). The external-beam setup was developed as an end-stage of the in-vacuum setup using an exit nozzle with a 1 mm wide and 100 nm thick Si_3N_4 window. The beam spatial resolution is then $60 \times 70 \mu\text{m}^2$ while maintaining the beam scanning capabilities.

With the external beam setup, it is possible to analyse the elemental composition (in point, line or areal map modes) and perform structural studies of different objects, independently of the size, using IBA techniques in both, open air or helium rich atmosphere [2]. An ion beam-induced luminescence (IBIL) setup using a TRIAX190 spectrometer is coupled to the chamber allowing the collection of radiation emitted in the range from 200 to 1100 nm. The experimental chamber has recently been upgraded with an improved light collection system



Fig. 2 Experimental chamber dedicated to study large and contaminated materials with tritium and beryllium from fusion reactors

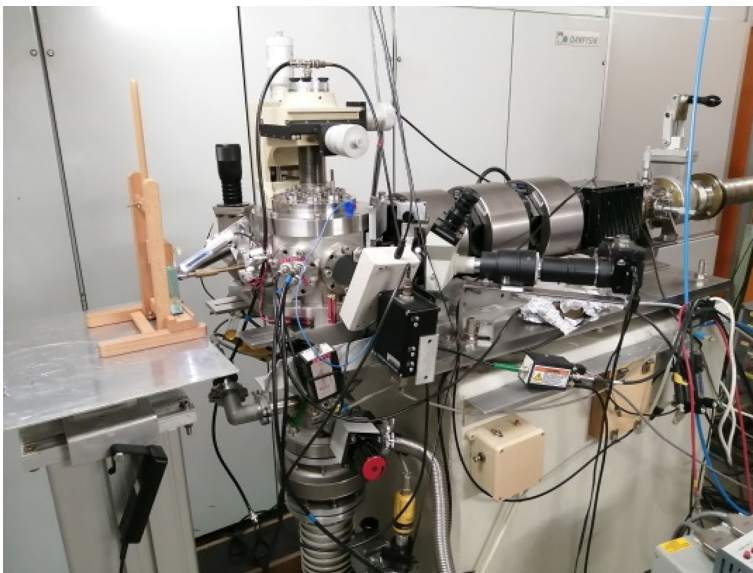


Fig. 3 Scanning Nuclear Microprobe based on the OM150 system developed by Oxford Microbeams. The external ion microbeam analytical end-station is also shown

as well as a setup for in situ electrical measurements allowing, in addition to RBS and PIXE analysis, the monitoring of the IBIL and the effect of radiation on electrical properties of materials and devices [3]. Some special applications of this system will be explored in the next paragraphs. The set-up can alternatively be installed at the 3 MV Tandem accelerator. Despite losing the lateral spatial resolution and mapping facility, the Tandem offers the possibility to

perform in situ irradiation measurements at higher energies and using heavy ions such as C, N and O besides protons and alpha particles.

The 3 MV Tandem is equipped with a Duoplasmatron H⁻ source and a SNICS sputtering source with a Li channel for He-beams. A micro-AMS system and 3 further experimental lines are installed: A multipurpose IBA chamber for RBS, PIXE, NRA (nuclear reaction analysis) and PIGE (particle induce gamma emission), a high-resolution PIXE system [4] and a line for Nuclear Physics experiments shared with the Nuclear Physics group of NOVA University of Lisbon, Fig. 1.

The micro-AMS system is based on a microbeam chamber connected to a General Ionex Model 834 HICONEX ion source modified so that it can focus the primary Cs⁺ beam in very small areas on the target (down to a few μm) [5]. The target plate is attached to a XYZ sample stage that allows movement in 0.5 μm steps and can take up to 3 targets with 25 mm diameter each. The secondary beam produced in the microbeam chamber is injected in the low energy beam line that features several focusing and deflecting devices and a 90° bend mass spectrometer with a beam product of 140 MeV·amu. At the high-energy side of the system there is a 90° double focusing mass analyser produced by Danfysik, corrected to the second order with a nominal maximum beam product (mE/q^2) of 140 MeV/amu, although it can work up to 10% above the specifications, which allows for analysis of mass 240 at 15 MeV (5+ charge state at 2.5 MV terminal voltage). The bouncing system allows for the quasi-simultaneous injection of different isotopes, therefore assuring high precision isotopic ratio measurement. It can switch between isotopes at a very high time rate (keeping the switching time below 100 ms/isotope) by applying an electric field that deflects the beam while keeping the magnetic field fixed. It does so in both the low energy magnet, by applying voltages directly to the magnet beam box, and in the high-energy magnet by applying voltages to two pairs of deflector plates, one at the entrance and another one at the exit of the high-energy magnet.

The micro-AMS system is especially tuned for high mass elements such as Pb, U, Th, where applications in the fields of geology (²³⁶U), archaeology (Pb isotopes), environmental sciences (²³⁶U in groundwater samples), nuclear safeguards (²³⁶U, ²³⁹Pu, ²³⁷Np) and astrophysics (¹⁸²Hf, ²⁴⁴Pu), amongst others, can be explored.

The High-Resolution High Energy PIXE [6] (2008) installation is among the few in the world offering the possibility to measure PIXE spectra covering an energy range of about 1 keV to 120 keV, with a relative resolution better than 1.5%. The full range is achieved using a CdTe detector, operational for energies above 3.3 keV, complemented by a first generation transition edge sensor, TES, X-ray Microcalorimeter Spectrometer (XMS), capable of providing better than 1% relative resolution from below 1.0 keV up to 20 keV.

The high flux 210 kV ion implanter, model S1090 from Danfysik, is equipped with two ion sources, a sputtering and a Hoven type source. The versatility of both ion sources offers the possibility to implant all the stable elements in the periodic table. A homemade sample stage allows temperature controlled implantations in the range from 77 to 1273 K. A set of decelerating lenses makes possible implantations down to 1 keV energy. The implanter is connected to the RBS chamber of the Van de Graaff accelerator allowing implantation and in situ analysis.

In addition, the laboratory owns two X-ray diffractometers, a commercial D8 Discover Bruker-AXS high-resolution diffractometer equipped with GID facility allowing Grazing Incidence and Small Angle X-Ray Scattering, indicated for nanostructure analysis, and an in-house assembled X-ray diffractometer with a high power Rigaku 18 kW X-ray generator with a high-temperature sample stage (1300 K) for in situ measurements and a MBraun position sensitive detector.

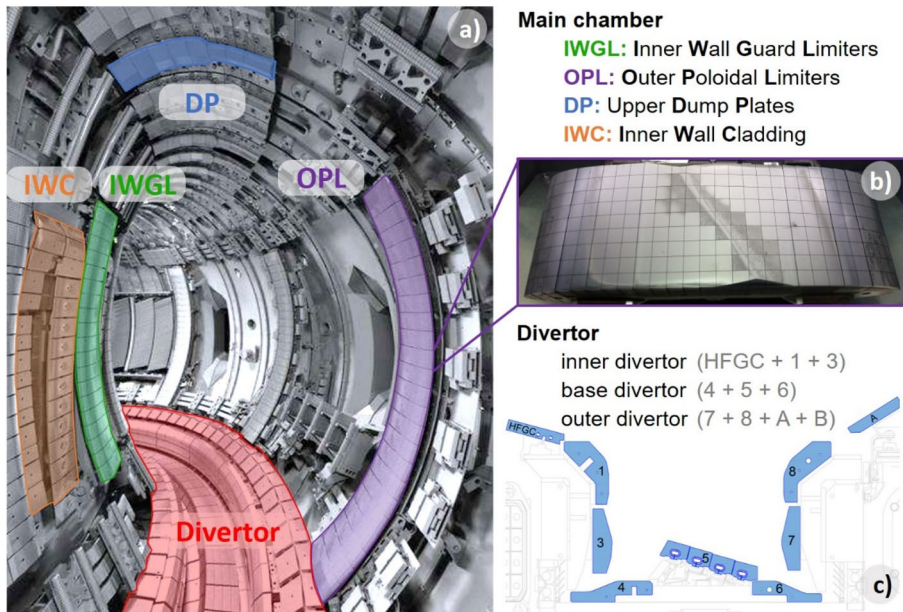


Fig. 4 **a** Image of the JET chamber identifying all the metallic wall zones; **b** example of a full tile from the outer limiter; **c** detailed scheme of the divertor

Finally, there is a pilot ^{60}Co irradiation unit with a current activity of 115 kCi with capacity for irradiation of industrial products and material irradiation studies.

3 Accelerator-based techniques and application

3.1 Ion beam techniques for advanced materials and cultural heritage studies

(a) Materials for fusion reactors

Plasma facing materials in the reactor chamber of fusion devices are submitted to heavy loads of radiation and heat which induce severe damage leading to drastic changes in their properties. Among the most important processes are erosion/redeposition and fuel retention in first wall materials. Also the presence of 14.1 MeV neutrons from the fusion reactions causes a lot of damage and transmutation on W with the production of He which could stabilise in bubbles inside the materials influencing their mechanical properties. To study these processes, accelerator-based techniques are ideal, providing information on the composition of the affected areas. LATR is the unique laboratory in the EUROfusion programme with a dedicated chamber (Fig. 2) to study full tiles contaminated with tritium and beryllium exposed in tokamaks, namely JET with the ITER-like wall configuration, Fig. 4 [7].

The different configurations of the plasma during the operations lead to significant differences and inhomogeneity in the interaction areas, even in the same tile. This poses great challenges to ion beam techniques pushing them to the limits. In Fig. 5 we show the results obtained for tile 4 of the divertor, exposed to a wide variety of plasma operating conditions.

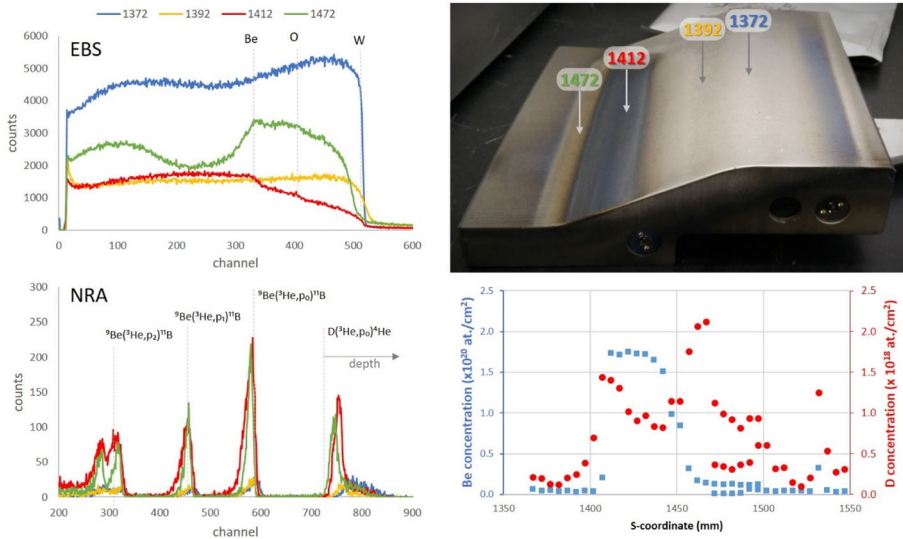


Fig. 5 Left: Elastic backscattering spectra (top) and nuclear reaction analysis (bottom) of different positions of tile 4, shown on top right. On the bottom right, beryllium and deuterium distribution on the surface of the tile

The tile was measured along the centre in a horizontal direction and some examples of the Elastic Backscattering Spectrometry (EBS) and NRA spectra collected are shown. The large number of points measured and the use of different techniques could only be processed with the NDF code [8] where all the data available are simultaneously analysed using the so-called total IBA analysis [9]. Despite the complexity of the deposits in the surface of the tile, we managed to extract the amount of Be and D deposited and have a clear understanding of the interaction processes.

Similar targeted IBA studies were performed for tiles placed in all the regions of the vessel providing the overall picture of the erosion/redeposition and fuel retention processes in JET [10–12] giving the necessary data to validate the models developed to describe plasma wall interactions.

Finally, another important issue is related with the damage and bubbles formation inside structural materials. Accelerators are unique to provide beams to mimic these processes in laboratory controlled conditions [13–15]. In Fig. 6 we show a SEM image of a high entropy alloy irradiated with Ar ions to study the damage evolution and bubble formation.

The equiatomic CuCrFeTiV sample was prepared by spark plasma sintering (SPS) and irradiated at room temperature with 300 keV Ar⁺ beam in the 3×10^{15} to 3×10^{18} ions/cm² fluence range in order to simulate the irradiation damage in the material. The microstructure observations at the surface revealed the existence of blistering in the samples irradiated with fluences of 3×10^{18} to Ar/cm² with feature diameters less than 1 μm. Moreover, cross-sectional scanning transmission electron microscopy data (not shown) reveal the presence of intergranular cavities and intragranular nanometric bubbles.

(b) Research on wide band gap semiconductors

Wide band gap semiconductors (WBS) such as group-III nitrides and metal oxides are key materials in novel electronic devices ranging from photonics to high power electronics and sensors [16]. GaN, AlN, InN and their ternary and quaternary compounds became famous

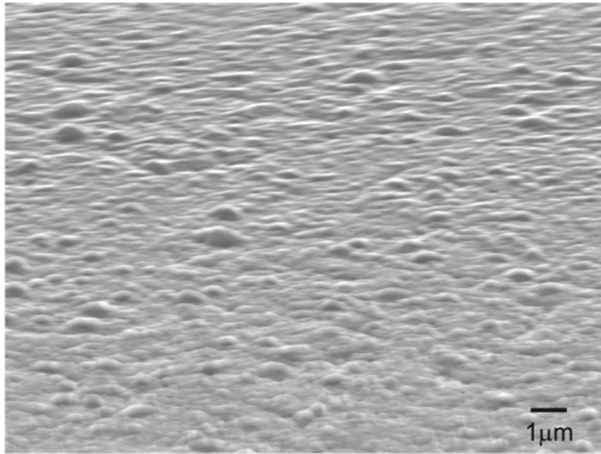


Fig. 6 SEM image of the surface of a CuCrFeTiV sample irradiated with 300 keV Ar ions (3×10^{18} ions/cm²)

due to their application in light emitting diodes (LEDs) and laser diodes for lighting and data storage [17]. Less known but equally promising is their potential for high-temperature, high power, high frequency and radiation resistant electronic devices, for example AlGaN and AlInN high electron mobility transistors. III-nitrides are expected to outperform silicon power devices concerning speed, breakdown voltage and on-resistance, opening the possibility of huge energy savings. Oxide semiconductors such as the MgZnO system and Ga₂O₃ are less mature in terms of device applications than III-nitrides, but they are handled as serious competitors to established technologies for optoelectronics and high power devices, respectively.

1. Thin film analysis and ion implantation

At LATR, RBS/Channelling (RBS/C) is used to study the composition and structural properties of WBS single crystals and thin films. Figure 7 shows RBS/C results of a ~ 100 nm thick Al_{86.8}In_{13.2}N layer grown epitaxially on a GaN buffer layer [18]. Random RBS spectra allow determining the composition directly, without the use of any standards and with depth resolution. In AlInN alloys, these measurements were important to assess homogeneity, auto-incorporation of Ga and the validity of Vegard's law [19–22]. Ion channelling measurements furthermore provide a quick quantification of the crystalline quality via the minimum yield χ_{\min} (the ratio between the yield in the aligned and the random spectrum). Minimum yield analysis is very versatile allowing quantitative comparison of crystal quality in bulk crystals and nanostructures such as quantum wells and even quantum dots, as well as quantification of implantation damage build-up [23–25]. Furthermore, full angular scans give information on strain in heteroepitaxial films. Figure 1b shows channelling scans across an oblique crystal axis for the thin film (In-signal) and the buffer layer (Ga-signal). The angular shift between the minima of these two curves is directly related with the strain state of the AlInN layer. However, care has to be taken since steering effects of the ion beam across the film/buffer interface can severely affect the final channelling pattern. These steering effects are responsible for the double-dip structure of the Ga-scan in Fig. 7b and even affect the magnitude of the measured angular shift. Monte Carlo simulations using the FLUX code [26] (lines in Fig. 7b) were used for a correct analysis of such data [17]. Further accuracy enhancement is achieved using position sensitive detectors acquiring full bidimensional blocking patterns [27].

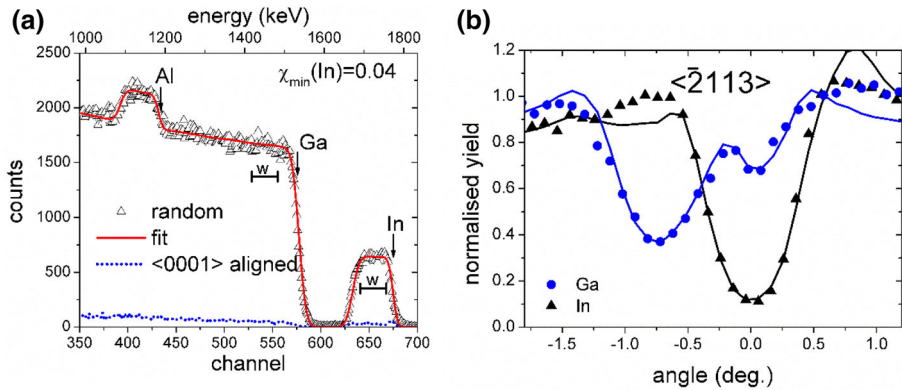


Fig. 7 **a** RBS/C random and $\langle 0001 \rangle$ -aligned spectra of an $\text{Al}_{86.8}\text{In}_{13.2}\text{N}/\text{GaN}$ sample taken with a 2 MeV He^+ beam and the fit to the random spectrum performed using the NDF [8] code. Also indicated are the windows (w) used for the angular scans in **b**. **b** Experimental angular scans (symbols) for Ga and In across the $\langle 2113 \rangle$ -axis and Monte Carlo simulations (lines) [17]

Another powerful application of ion channelling in combination with Monte Carlo simulations is the measurement of the lattice site location of impurities. Extensive work on the lattice site location of rare earth ions in III-nitrides has been performed showing that these optically active ions are preferentially incorporated on substitutional group-III sites. However, considerable displacements can occur due to clustering or interaction with defects, in particular, for ion-implanted samples [28–30].

Monte Carlo simulations also allow de-convoluting the effect of different types of defects in RBS/C spectra of ion implanted samples [31]. Recently, Molecular Dynamics (MD) simulations were employed to understand radiation effects in GaN upon swift heavy ion irradiation. The developed simulation model shows exceptional agreement with experiments and RBS/C spectra were successfully simulated directly from the MD cell [32].

2. In situ characterisation of radiation sensors

The high radiation resistance of many WBS makes them promising materials for the next generation of radiation tolerant electronics for use in space and other radiation environments or as radiation detectors. The new up-grade of the experimental chamber at the microprobe permits a detailed real time analysis of ion irradiation effects on optical and electrical properties of materials and devices.

Figure 8a shows IBIL spectra obtained during proton irradiation of a thin flake of Ga_2O_3 produced by mechanical exfoliation. Ga_2O_3 is characterised by a large band gap of 4.9 eV. This example clearly elucidates the potential of using IBIL to complement conventional optical characterisation. For the characterisation of ultra-WBS, light sources for excitation above the band gap are limited in terms of energy, excitation density and penetration depth. Another relevant advantage comparatively to photoluminescence (PL) and cathodoluminescence (CL) is the possibility of monitoring the effect of irradiation in real time. Indeed, a clear reduction of the luminescence yield occurs during proton irradiation in Ga_2O_3 , as shown in Fig. 8a [3]. Figure 8b shows a transient study of the ion beam-induced current in a Metal–Semiconductor–Metal device based on Ga_2O_3 . When irradiating the Schottky contact operating in reverse bias, a clear ionic current is observed, showing that the device operates as an efficient radiation sensor. Furthermore, these studies with spatial resolution using the microprobe allow studying how the irradiation of specific regions affects the overall device

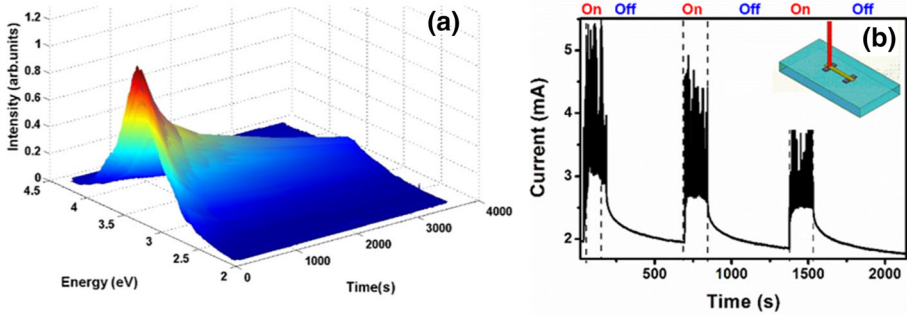


Fig. 8 **a** IBIL evolution during irradiation with a flux of 3.12×10^{12} protons/s.cm². **b** Transient measurements of the ionocurrent induced when irradiating the reverse biased Schottky contact of a Ga₂O₃ MSM device. The in-set shows the schematic of the MSM structure under irradiation

performance. Besides Ga₂O₃, such in situ electrical characterisation was also applied to study devices based on GaN and MoO₃ microstructures.

(c) Studies of cultural heritage artefacts using an external high energetic particle beam

The study of ancient artefacts composition allows determining the raw materials used and their production techniques which is quite important for the characterisation of cultural heritage (CH) artefacts providing clues for their provenance and at the same time contributing to establish their authenticity. Counterfeiting of CH artefacts is nowadays a global problem that is being tackled with the use of powerful methods and techniques as may be ascertained by the ongoing IAEA CRP F11021 *Enhancing Nuclear Analytical Techniques to Meet the Needs of Forensic Sciences* with applications to CH materials.

The external-beam setup allows the study of a wide range of materials and objects being ideal for the characterisation of CH samples profiting from the non-destructive and high sensitivity capabilities of IBA techniques. A wide range of collaborations with private collectors, museums, universities and other entities related to the CH field has been established. The objects analysed along these years cover a wide range of materials and different studies such as golden and silver artefacts belonging to National Treasure, coins belonging to important and unique collections [33], bronze and copper artefacts [34], paintings, glass, stained glass, glazed tiles ceramics, and old manuscripts written with iron gall inks [35].

The studies cover, for example, composition analysis, surface elemental distribution and depth profile [2], corrosion distribution and composition [40], or radiation damage evaluation in some heritage materials, Figs. 9, 10, 11.

Paintings on copper plates have a very thin pictorial layer (50–100 μm) and because of that their characterisation by means of IBA is very adequate to study the pigments in a non-destructive way [41]. The paintings, attributed to Frans Francken II (1605–1645), were analysed using the external-beam setup (Fig. 11) with the aim of studying the used colour palette composition. In Fig. 11b) some of the X-ray spectra recorded for the different pigments are shown.

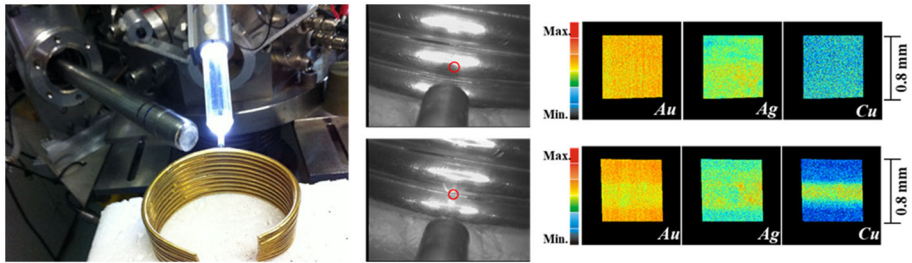


Fig. 9 Analysis of a Late Bronze Age gold bracelet from the collection of the National Museum of Archaeology consisting of 10 rods that were found to be joined by using 5 Cu-rich gold solder alloys with slightly different melting points [36]

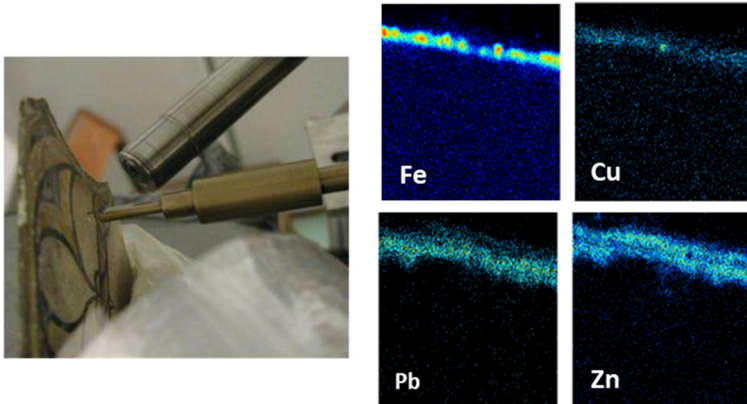


Fig. 10 Study of historical glass and stained glass. From raw materials to production techniques [37–39]. This figure shows $264 \times 264 \mu\text{m}^2$ elemental distribution maps on a cross-section view of a stained glass with a surface paint layer of grisaille

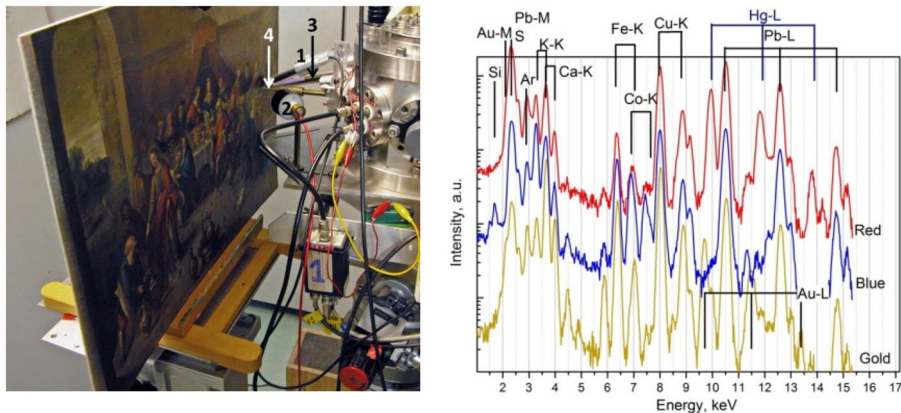


Fig. 11 Photography taken during the experiments: **a** 1. Video Camera; 2. Particle detector; 3. X-ray detector; 4. Exit nozzle; **b** X-ray spectra recorded for different colours of the paintings studied: red showing the presence of Hg and S (vermillion), blue presenting Pb, Cu, Fe and Co (cobalt smalt) and pigment containing gold [39]

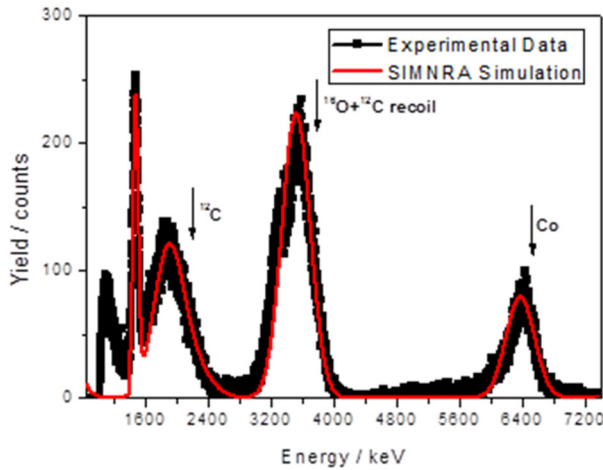


Fig. 12 Elastic reaction spectrum for 8 MeV of $^{16}\text{O}^{3+}$ for $\theta_{\text{lab}} = 45^\circ$

3.2 Nuclear reactions

(a) Astrophysics

Nuclear Reaction work is aimed at two main objectives: 1. The measurement of nuclear reactions relevant to Nuclear Physics and to Nuclear Astrophysics; and 2. The development of PIGE through measurement of the cross sections of the relevant gamma-producing nuclear reactions and development of methodologies and software for PIGE and its applications.

Regarding Nuclear Astrophysics full advantage has been taken of the different installed facilities. The interesting part of the excitation function lies in the low energy part range where cross sections are below the micro-barn range, leading to the need of very pure and stable targets that can withstand high-current beams.

Hence, the 210 kV implanter was used to produce ^{14}N targets for the measurement of the reaction $^{14}\text{N}(p,\gamma)^{15}\text{O}$ [42] within the LUNA collaboration at Gran Sasso and also ^{16}O targets for the measurement of $^{16}\text{O} + ^{16}\text{O}$ reactions [43, 44]. Results for the elastic scattering reactions $^{12}\text{C} + ^{16}\text{O}$ and $^{16}\text{O} + ^{16}\text{O}$ were obtained at the nuclear reaction line of the tandem accelerator (see Fig. 12).

Also in connection to Nuclear Astrophysics, the AMS line of the tandem accelerator was used to measure the cross section of the reaction $^{35}\text{Cl}(n,\gamma)^{36}\text{Cl}$. ^{36}Cl has a half-life of 3.01×10^5 y, implying that the amount of ^{36}Cl existing at the earth soil may only be explained by continuous production in the sun wind or bombardment of the earth surface by cosmic neutrons. The targets were obtained by the bombardment of ^{35}Cl by thermal neutrons and their content of ^{36}Cl was quantified by AMS, leading to a cross section value that, within the uncertainties, is in agreement with the average of previous published results [45].

Measurement of elastic scattering of protons, namely the reactions $^6\text{Li}(p,p)^6\text{Li}$, $^7\text{Li}(p,p)^7\text{Li}$, $^{12}\text{C}(p,p)^{12}\text{C}$, $^{19}\text{F}(p,p)^{19}\text{F}$, $^{31}\text{P}(p,p)^{31}\text{P}$, at forward and backward angles, where there is little data available, can provide reliable information both for obtaining accurate optical model parameters as well as for the characterisation of excited states of nuclides. A theoretical analysis fitted to the results is ongoing using Azure software (see Fig. 13).

In relation to PIGE and measurement of cross sections of gamma-producing nuclear reactions, the work produced since 2000 culminated in an IAEA concerted research project

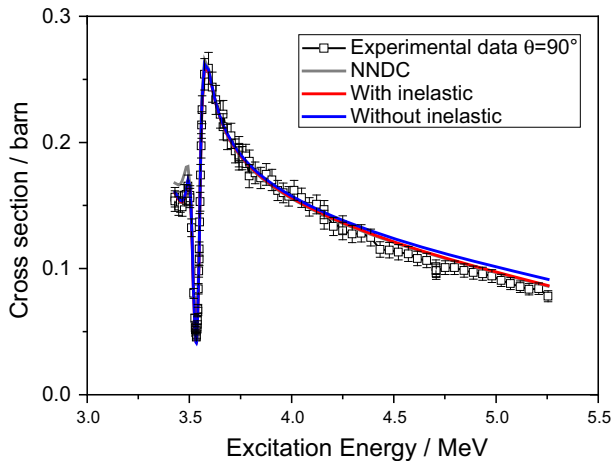


Fig. 13 $^{12}\text{C}(p,p)^{12}\text{C}$ experimental cross section and theoretical simulation using the Azure code

Development of a Reference Database for Particle Induced Gamma Ray Emission (PIGE) Spectroscopy [46]. The objective of that project was the gathering from the literature and the measurement of missing cross sections of gamma-producing nuclear reactions in light isotopes, being the results assembled in the IBANDL database. A few papers followed this effort [47–51].

In parallel, development of methodologies and software for PIGE was accomplished. Software for standard-free PIGE bulk analysis, ERYA Bulk, was created. The most recent version was tested within a systematic inter-comparison of PIGE data analysis codes, initiated by the IAEA in 2018 [52, 53].

In order to deal with in-depth heterogeneous samples, a code for PIGE profiling analysis, ERYA Profiling, was developed. ERYA profiling has the capacity to perform a full straggling calculation with Landau, Vavilov or Gaussian distributions, and use as input relevant PIGE excitation functions combined or not with Breit–Wigner resonances and resonance strengths. Cross sections measurement of proton inelastic scattering from ^{19}F and ^{31}P , together with the standard-free methodology based on the ERYA bulk code, promoted biomedical applications. Elemental analysis of bone samples affected by Osteoporosis and Paget’s Disease of Bone was performed. A biomarker related to Zn concentrations versus the ratio of P/Ca is strongly suggested by the results [54]. Further recent analyses of PIGE spectra have enlightened the role of light elements, namely F.

(b) Fusion relevant cross sections

The impact of ion beam techniques in fusion raised the importance to have reliable nuclear reactions cross sections to use in the software codes to analyse the data, namely SIMNRA [55, 56] and NDF [8]. The cross sections for two relevant materials in fusion devices, Be and Li, are particularly disperse with several gaps in the data base. One example is the $^9\text{Be}(^3\text{He},p_x)^{11}\text{B}$ reaction, the lower-energy peaks cannot be simulated due to missing cross-section data and the higher energy peaks are only known for some energies and scattering angles [57, 58]. We measured the $^9\text{Be}(^3\text{He},p_i)^{11}\text{B}$ cross section for $i = 0, 1, 2, 3$ at an angle of 135° in the energy range 0.7–2.5 MeV [59]. We used two different thin films with different Be thickness, and also a bulk sample together with a fitting method. The results obtained

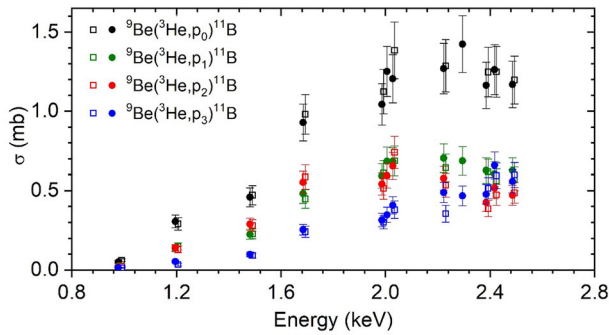


Fig. 14 ${}^9\text{Be}({}^3\text{He}, \pi_i){}^{11}\text{B}$ cross sections for $i = 0, 1, 2, 3$ determined in [59]. The square symbols are the results from the Be 25 nm thin films and circles symbols are for 50 nm thin films

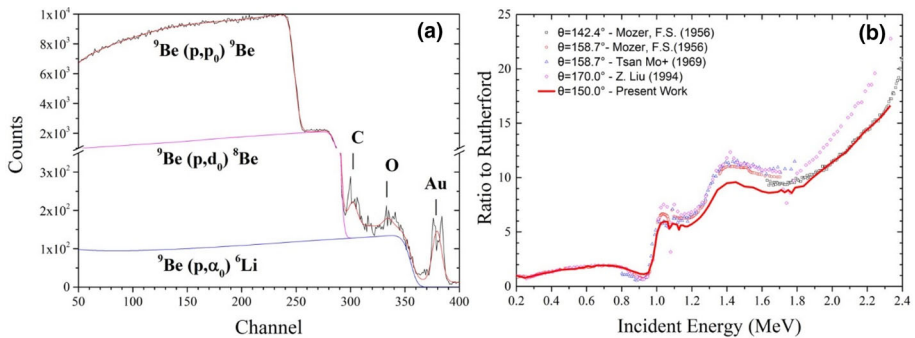


Fig. 15 **a** Typical EBS and nuclear reaction spectrum for 2.23 MeV incident protons onto the Be target. Incident angle is 0° ; scattering angle is 150° . The contribution of each particle that reaches the detector is labelled; **b** ${}^9\text{Be}(p, \pi_0){}^9\text{Be}$ cross sections at 150° compared with results from literature

with the three different samples and two methods all agree with each other for the ground state and for the three excited states accessed, Fig. 14.

In order to investigate beryllium migration, which connects the lifetime of first-wall components under erosion with tokamak safety, EBS is often employed for depth profiling. Besides the backscattering, there are two nuclear reactions of protons with ${}^9\text{Be}$ that we should consider: ${}^9\text{Be}(p, d_0){}^8\text{Be}$ and ${}^9\text{Be}(p, \alpha_0){}^6\text{Li}$. In the case of nuclear reactions, the data available is more limited than for backscattering. The ${}^9\text{Be}(p, d_0){}^8\text{Be}$ reaction has a relatively large cross section in the energy range 1–2.5 MeV and must be considered for accurate measurement. We measured the ${}^9\text{Be}(p, \pi_0){}^9\text{Be}$, ${}^9\text{Be}(p, d_0){}^8\text{Be}$ and ${}^9\text{Be}(p, \alpha_0){}^6\text{Li}$ cross sections in the energy range 0.5–2.35 MeV, at an angle of 150° [60]. The use of this new cross section shows that the Au, O, C and Al peaks are well separated from the ${}^9\text{Be}(p, d_0){}^8\text{Be}$ and ${}^9\text{Be}(p, \alpha_0){}^6\text{Li}$ reaction and the ${}^9\text{Be}(p, \pi_0){}^9\text{Be}$ backscattering plateaus, Fig. 15a.

The differential cross section for ${}^9\text{Be}(p, \pi_0){}^9\text{Be}$ in the laboratory system is shown in Fig. 15b. We got a good agreement of the shape of the cross section with the reference data; the resonances are in the same proton energies. However, for energies above 1 MeV the absolute values differ, albeit by less than 15%.

4 Conclusion

Ion beam laboratories and accelerators of all types (electrostatic, cyclotrons, linear, etc.) and energy ranges play and will keep playing a leading role in the future of technological development and fundamental research. New applications, like single ion implantation, will bring quantum technologies into the well-established ion beam world. Quantum technologies or production of new isotopes for medical applications are just two examples of emerging application of ion beam technologies. Our work at LATR, covering a broad range of applications and sciences, is a clear evidence of the importance of accelerators on nowadays life. The role of small–medium size laboratories is essential to teach and train the future generations in accelerator technology and science, exploring and developing new applications for ion beam technologies.

Acknowledgements We acknowledge Rui Silva, Carlos Cruz, Jorge Rocha and Hélio Luís for valuable contributions to maintain the Laboratory in good operating conditions all these years. Special thanks to public and private museums and entities which allow us to characterise invaluable objects. We acknowledge funding by FCT, Portugal in various individual and project grants, as well as by the EC and IAEA.

References

1. L.C. Alves, M.B.H. Breese, E. Alves, A. Paúl, M.R. da Silva, M.F. da Silva, J.C. Soares, Micron-scale analysis of SiC/SiCf composites using the new Lisbon nuclear microprobe. *Nucl. Inst. Methods Phys. Res. Sect. B Beam Interact. Mater. Atoms* **1**, 334–338 (2000)
2. V. Corregidor, L.C. Alves, N.P. Barradas, M.A. Reis, M.T. Marques, J.A. Ribeiro, Characterization of mercury gilding art objects by external proton beam. *Nucl. Instrum. Methods Phys. Res. Sect. B Beam Interact. Mater. Atoms* **269**, 3049–3053 (2011). <https://doi.org/10.1016/j.nimb.2011.04.070>
3. M. Peres, L.C. Alves, F. Rocha, N. Catarino, C. Cruz, E. Alves, A.G. Silva, E.G. Vllora, K. Shimamura, K. Lorenz, In situ characterization and modification of β -Ga₂O₃ flakes using an ion micro-probe. *Phys. Status Solidi* **215**, 1800190 (2018). <https://doi.org/10.1002/pssa.201800190>
4. P.C. Chaves, A. Taborda, J.P. Marques, M.A. Reis et al., PIXE spectra obtained at the high resolution high energy PIXE setup. *Nucl. Instruments Methods Phys. Res. Sect. B Beam Interact. Mater. Atoms* **318**, 60–64 (2014). <https://doi.org/10.1016/j.nimb.2013.05.100>
5. S.H. Sie, T.R. Niklaus, G.F. Suter, Microbeam AMS: prospects of new geological applications. *Nucl. Instrum. Methods Phys. Res. Sect. B Beam Interact. Mater. Atoms* **123**, 112–121 (1997). [https://doi.org/10.1016/S0168-583X\(96\)00417-X](https://doi.org/10.1016/S0168-583X(96)00417-X)
6. M.A. Reis, P.C. Chaves, A. Taborda, Review and perspectives on energy dispersive high resolution PIXE and RYIED. *Appl. Spectrosc. Rev.* **52**, 231–248 (2017). <https://doi.org/10.1080/05704928.2016.1226181>
7. M. Mayer, S. Möller, M. Rubel, A. Widdowson, S. Charisopoulos, T. Ahlgren, E. Alves, G. Apostolopoulos, N.P. Barradas, S. Donnelly, S. Fazinić, K. Heinola, O. Kakuee, H. Khodja, A. Kimura, A. Lagoyannis, M. Li, S. Markelj, M. Mudrinic, P. Petersson, I. Portnykh, D. Primetzhofer, P. Reichart, D. Ridikas, T. Silva, S.M. Gonzalez de Vicente, Y.Q. Wang, Ion beam analysis of fusion plasma-facing materials and components: facilities and research challenges. *Nucl. Fusion* **60**, 025001 (2020). <https://doi.org/10.1088/1741-4326/ab5817>
8. N.P. Barradas, C. Jeynes, Advanced physics and algorithms in the IBA DataFurnace. *Nucl. Instrum. Methods Phys. Res. Sect. B Beam Interact. Mater. Atoms* **266**, 1875–1879 (2008). <https://doi.org/10.1016/j.nimb.2007.10.044>
9. C. Jeynes, V.V. Palitsin, G.W. Grime, C. Pascual-Izarra, A. Taborda, M.A. Reis, N.P. Barradas, External beam total-IBA using DataFurnace. *Nucl. Instrum. Methods Phys. Res. Sect. B Beam Interact. Mater. Atoms* **481**, 47–61 (2020). <https://doi.org/10.1016/j.nimb.2020.08.002>
10. A. Baron-Wiechec, A. Widdowson, E. Alves, C.F. Ayres, N.P. Barradas, S. Brezinsek, J.P. Coad, N. Catarino, K. Heinola, J. Likonen, G.F. Matthews, M. Mayer, P. Petersson, M. Rubel, W. van Renterghem, I. Uytendhouwen, Global erosion and deposition patterns in JET with the ITER-like wall. *J. Nucl. Mater.* **463**, 157–161 (2015). <https://doi.org/10.1016/j.jnucmat.2015.01.038>

11. N. Catarino, A. Widdowson, A. Baron-Wiechec, J.P. Coad, K. Heinola, M. Rubel, E. Alves, Time-resolved deposition in the remote region of the JET-ILW divertor: measurements and modelling. *Phys. Scr.* **T170**, 014059 (2017). <https://doi.org/10.1088/1402-4896/aa8c9a>
12. A. Widdowson, J.P. Coad, E. Alves, A. Baron-Wiechec, N.P. Barradas, S. Brezinsek, N. Catarino, V. Corregidor, K. Heinola, S. Koivuranta, S. Krat, A. Lahtinen, J. Likonen, G.F. Matthews, M. Mayer, P. Petersson, M. Rubel, Overview of fuel inventory in JET with the ITER-like wall. *Nucl. Fusion.* **57**, 086045 (2017). <https://doi.org/10.1088/1741-4326/aa7475>
13. R. Mateus, M. Dias, J. Lopes, J. Rocha, N. Catarino, N. Franco, V. Livramento, P.A. Carvalho, J.B. Correia, K. Hanada, E. Alves, Effects of helium and deuterium irradiation on SPS sintered W-Ta composites at different temperatures. *J. Nucl. Mater.* **442**, S251–S255 (2013). <https://doi.org/10.1016/j.jnucmat.2013.02.068>
14. M. Dias, R. Mateus, N. Catarino, N. Franco, D. Nunes, J.B. Correia, P.A. Carvalho, K. Hanada, C. Sárbu, E. Alves, Synergistic helium and deuterium blistering in tungsten–tantalum composites. *J. Nucl. Mater.* **442**, 69–74 (2013). <https://doi.org/10.1016/j.jnucmat.2013.08.010>
15. N. Catarino, L.C. Alves, M. Dias, N.P. Barradas, S. van Til, M. Zmitko, E. Alves, Oxidation behaviour of neutron irradiated Be pebbles. *Nucl. Mater. Energy.* **23**, 100748 (2020). <https://doi.org/10.1016/j.nme.2020.100748>
16. S. Fujita, Wide-bandgap semiconductor materials: For their full bloom. *Jpn. J. Appl. Phys.* **54**, 030101 (2015). <https://doi.org/10.7567/JJAP.54.030101>
17. The Nobel Prize in Physics 2014 - NobelPrize.org, (n.d.). <https://www.nobelprize.org/prizes/physics/2014/summary/>. Accessed December 20, 2020.
18. K. Lorenz, N. Franco, E. Alves, I.M. Watson, R.W. Martin, K.P. O'Donnell, Anomalous ion channeling in AlInN/GaN bilayers: determination of the strain state. *Phys. Rev. Lett.* **97**, 085501 (2006). <https://doi.org/10.1103/PhysRevLett.97.085501>
19. M.D. Smith, E. Taylor, T.C. Sadler, V.Z. Zubialevich, K. Lorenz, H.N. Li, J. O'Connell, E. Alves, J.D. Holmes, R.W. Martin, P.J. Parbrook, Determination of Ga auto-incorporation in nominal InAlN epilayers grown by MOCVD. *J. Mater. Chem. C.* **2**, 5787–5792 (2014). <https://doi.org/10.1039/c4tc00480a>
20. A. Redondo-Cubero, K. Lorenz, R. Gago, N. Franco, M.A. Difortepoisson, E. Alves, E. Muñoz, Depth-resolved analysis of spontaneous phase separation in the growth of lattice-matched AlInN. *J. Phys. D: Appl. Phys.* (2010). <https://doi.org/10.1088/0022-3727/43/5/055406>
21. K. Lorenz, N. Franco, E. Alves, S. Pereira, I.M. Watson, R.W. Martin, K.P. O'Donnell, Relaxation of compressively strained AlInN on GaN. *J. Cryst. Growth.* **310**, 4058–4064 (2008). <https://doi.org/10.1016/j.jcrysgro.2008.07.006>
22. S. Magalhães, N. Franco, I.M. Watson, R.W. Martin, K.P. O'Donnell, H.P.D. Schenk, F. Tang, T.C. Sadler, M.J. Kappers, R.A. Oliver, T. Monteiro, T.L. Martin, P.A.J. Bagot, M.P. Moody, E. Alves, K. Lorenz, Validity of Vegard's rule for $\text{Al}_{1-x}\text{In}_x\text{N}$ (0.08 < x < 0.28) thin films grown on GaN templates. *J. Phys. D: Appl. Phys.* **50** (2017) 205107. <https://doi.org/10.1088/1361-6463/aa69dc>
23. A. Redondo-Cubero, K. Lorenz, E. Wendler, D. Carvalho, T. Ben, F.M. Morales, R. García, V. Fellmann, B. Daudin, Selective ion-induced intermixing and damage in low-dimensional GaN/AlN quantum structures. *Nanotechnology* **24**, 505717 (2013). <https://doi.org/10.1088/0957-4484/24/5/050717>
24. K. Lorenz, E. Wendler, A. Redondo-Cubero, N. Catarino, M.P. Chauvat, S. Schwaiger, F. Scholz, E. Alves, P. Ruterana, Implantation damage formation in a-, c- and m-plane GaN. *Acta Mater.* **123**, 177–187 (2017). <https://doi.org/10.1016/j.actamat.2016.10.020>
25. D.N. Faye, X. Biquard, E. Nogales, M. Felizardo, M. Peres, A. Redondo-Cubero, T. Auzelle, B. Daudin, L.H.G. Tizei, M. Kociak, P. Ruterana, W. Möller, B. Méndez, E. Alves, K. Lorenz, Incorporation of Europium into GaN Nanowires by Ion Implantation. *J. Phys. Chem. C.* **123**, 11874–11887 (2019). <https://doi.org/10.1021/acs.jpcc.8b12014>
26. P.J.M. Smulders, D.O. Boerma, Computer simulation of channeling in single crystals. *Nucl. Inst. Methods Phys. Res. B.* **29**, 471–489 (1987). [https://doi.org/10.1016/0168-583X\(87\)90058-9](https://doi.org/10.1016/0168-583X(87)90058-9)
27. A. Redondo-Cubero, E. David-Bosne, U. Wahl, P. Miranda, M.R. Da. Silva, J.G. Correia, K. Lorenz, Strain detection in crystalline heterostructures using bidimensional blocking patterns of channelled particles. *J. Phys. D: Appl. Phys.* **51**, 115304 (2018). <https://doi.org/10.1088/1361-6463/aaad8b>
28. K. Lorenz, E. Alves, I.S. Roqan, K.P. O'Donnell, A. Nishikawa, Y. Fujiwara, M. Boćkowski, Lattice site location of optical centers in GaN: Eu light emitting diode material grown by organometallic vapor phase epitaxy. *Appl. Phys. Lett.* **97**, 111911 (2010). <https://doi.org/10.1063/1.3489103>
29. E. Alves, K. Lorenz, R. Vianden, C. Boemare, M.J. Soares, T. Monteiro, Optical doping of nitrides by ion implantation. *Mod. Phys. Lett. B.* **15**, 1281–1287 (2001). <https://doi.org/10.1142/S0217984901003172>

30. M. Fialho, J. Rodrigues, S. Magalhães, M.R. Correia, T. Monteiro, K. Lorenz, E. Alves, Effect of AlN content on the lattice site location of terbium ions in $Al_xGa_{1-x}N$ compounds. *Semicond. Sci. Technol.* **31**, 035026 (2016). <https://doi.org/10.1088/0268-1242/31/3/035026>
31. P. Jozwik, L. Nowicki, R. Ratajczak, A. Stonert, C. Mieszczynski, A. Turos, K. Morawiec, K. Lorenz, E. Alves, Monte Carlo simulations of ion channeling in crystals containing dislocations and randomly displaced atoms. *J. Appl. Phys.* **126**, 195107 (2019). <https://doi.org/10.1063/1.511619>
32. M.C. Sequeira, J.-G. Mattei, H. Vazquez, F. Djurabekova, K. Nordlund, I. Monnet, P. Mota-Santiago, P. Kluth, C. Grygiel, S. Zhang, E. Alves, K. Lorenz, Unravelling the secrets of the resistance of GaN to strongly ionising radiation. *Commun. Phys.* **4**, 51 (2021). <https://doi.org/10.1038/s42005-021-00550-2>
33. R. Borges, R. Silva, L. Alves, M. Araújo, A. Candeias, V. Corregidor, J. Vieira, European silver sources from the 15th to the 17th century: the influx of “new world” silver in Portuguese currency. *Heritage* **1**, 453–467 (2018). <https://doi.org/10.3390/heritage1020030>
34. P. Valério, I.P. Cardoso, M. Santiago, M.F. Araújo, L.C. Alves, M.A. Gonçalves, R. Mataloto, Microanalytical study of copper ores from the Chalcolithic settlement of São Pedro (Portugal): copper production in the south-western Iberian Peninsula. *Archaeometry* **62**, 314–328 (2020). <https://doi.org/10.1111/arc.12514>
35. V. Corregidor, R. Viegas, L.M. Ferreira, L.C. Alves, Study of iron gall inks, ingredients and paper composition using non-destructive techniques. *Heritage* **2**, 2691–2703 (2019). <https://doi.org/10.3390/heritage2040166>
36. L.C. Alves, V. Corregidor, Análise PIXE das bracelets de Cantonha e do Álamo, in *Ouvrivesaria Pré-Histórica Do Ocidente Penins. Atlântico Compreender Para Conserv.*, AuCORRE, Lisboa, 2014.
37. M. Vilarigues, C. Machado, A. Machado, M. Costa, L.C. Alves, I.P. Cardoso, A. Ruivo, Grisailles: reconstruction and characterization of historical recipes. *Int. J. Appl. Glas. Sci.* **11**, 756–773 (2020). <https://doi.org/10.1111/ijag.15793>
38. M. Vilarigues, I. Coutinho, T. Medici, L.C. Alves, B. Gratuze, A. Machado, From beams to glass: determining compositions to study provenance and production techniques. *Phys. Sci. Rev.* (2019). <https://doi.org/10.1515/psr-2018-0019>
39. I. Coutinho, T. Medici, L.C. Alves, B. Gratuze, M. Vilarigues, Provenance studies of 18th century potassium-rich archaeological glass from Portugal. *J. Archaeol. Sci. Rep.* **13**, 185–198 (2017). <https://doi.org/10.1016/j.jasrep.2017.03.050>
40. J. Cruz, M. Manso, V. Corregidor, R.J.C. Silva, E. Figueiredo, M.L. Carvalho, L.C. Alves, Surface analysis of corroded XV–XVI century copper coins by μ -XRF and μ -PIXE/ μ -EBS self-consistent analysis. *Mater. Charact.* **161**, 110170 (2020). <https://doi.org/10.1016/j.matchar.2020.110170>
41. V. Corregidor, A.R. Oliveira, P.A. Rodrigues, L.C. Alves, Paintings on copper by the Flemish artist Frans Francken II: PIXE characterization by external microbeam. *Nucl. Instrum. Methods Phys. Res. Sect. B Beam Interact. Mater. Atoms.* **348**, 291–295 (2015). <https://doi.org/10.1016/j.nimb.2014.12.072>
42. A. Lemut, D. Bemmerer, F. Confortola, R. Bonetti, C. Broggin, P. Corvisiero, H. Costantini, J. Cruz, A. Formicola, Z. Fülöp, G. Gervino, A. Guglielmetti, C. Gustavino, G. Gyürky, G. Imbriani, A.P. Jesus, M. Junker, B. Limata, R. Menegazzo, P. Prati, V. Roca, D. Rogalla, C. Rolf, M. Romano, C. Rossi Alvarez, F. Schümmer, E. Somorjai, O. Straniero, F. Strieder, F. Terrasi, H.P. Trautvetter, First measurement of the $^{14}N(p, \gamma)^{15}O$ cross section down to 70 keV. *Phys. Lett. Sect. B Nucl. Elem. Part. High Energy Phys.* **634**, 483–487 (2006). <https://doi.org/10.1016/j.physletb.2006.02.021>
43. H. Silva, J. Cruz, A.M. Sánchez-Benítez, C. Santos, H. Luís, M. Fonseca, A.P. Jesus, Production of thin targets by implantation for the measurement of the $^{16}O + ^{16}O$ elastic scattering below the Coulomb barrier. *Nucl. Instrum. Methods Phys. Res. Sect. B Beam Interact. Mater. Atoms.* **406**, 135–138 (2017). <https://doi.org/10.1016/j.nimb.2017.02.049>
44. H. Silva, J. Cruz, A. Redondo-Cubero, C. Santos, M. Fonseca, H. Luis, A.P. Jesus, Comparative analysis of anodized, implanted and sputtered tantalum oxide targets for the study of $^{16}O + ^{16}O$ fusion reaction. *Nucl. Instrum. Methods Phys. Res. Sect. B Beam Interact. Mater. Atoms.* **331**, 78–81 (2014). <https://doi.org/10.1016/j.nimb.2013.12.039>
45. H. Luís, A.P. Jesus, M. Fonseca, J. Cruz, D. Galaviz, N. Franco, E. Alves, Study of nuclear reactions producing ^{36}Cl by micro-AMS, in *Journal of Physics: Conference Series* (Institute of Physics Publishing, 2016), pp. 012077. <https://doi.org/10.1088/1742-6596/665/1/012077>
46. Development of a Reference Database for Particle Induced Gamma Ray Emission (PIGE) Spectroscopy, INTERNATIONAL ATOMIC ENERGY AGENCY, Vienna, 2017. <https://www.iaea.org/publications/12235/development-of-a-reference-database-for-particle-induced-gamma-ray-emission-pige-spectroscopy>
47. M. Chiari, B. Melon, L. Salvestrini, M. Fonseca, E. Alves, A.P. Jesus, Measurement of proton induced γ -ray emission cross sections on Al from 25 to 41 MeV. *Nucl. Instrum. Methods Phys. Res. Sect. B Beam Interact. Mater. Atoms.* **332**, 355–358 (2014). <https://doi.org/10.1016/j.nimb.2014.02.095>

48. P. Dimitriou, H.W. Becker, I. Bogdanović-Radović, M. Chiari, A. Goncharov, A.P. Jesus, O. Kakuee, A.Z. Kiss, A. Lagoyannis, J. Räisänen, D. Strivay, A. Zucchiatti, Development of a reference database for particle-induced gamma-ray emission spectroscopy. *Nucl. Instrum. Methods Phys. Res. Sect. B Beam Interact. Mater. Atoms.* **371**, 33–36 (2016). <https://doi.org/10.1016/j.nimb.2015.09.052>
49. P. Cabanelas, J. Cruz, M. Fonseca, A. Henriques, F. Lourenço, H. Luís, J. Machado, J. Pires Ribeiro, A.M. Sánchez-Benítez, P. Teubig, P. Velho, M. Zarza-Moreno, D. Galaviz, A.P. Jesus, Cross sections for proton induced high energy γ -ray emission (PIGE) in reaction $19\text{F}(p, \alpha\gamma)16\text{O}$ at incident proton energies between 15 and 4 MeV. *Nucl. Instrum. Methods Phys. Res. Sect. B Beam Interact. Mater. Atoms.* **381**, 110–113 (2016). <https://doi.org/10.1016/j.nimb.2016.06.003>
50. M. Chiari, E. Alves, I. Bogdanović Radović, J. Cruz, L. Csedreki, M. Fonseca, D. Galaviz, A. Henriques, M. Jakšić, A.P. Jesus, O. Kakuee, Z. Kiss, A. Lagoyannis, F. Lourenço, H. Luís, J. Machado, B. Melon, C.K. Nuviadenu, L. Salvestrini, N. Sharifzadeh, Z. Siketić, G. Sziki, Z. Szikszai, P. Teubig, P. Velho, I. Zamboni, M. Zarza, Measurement of proton induced γ -ray emission cross sections on Na from 1.0 to 4.1 MeV. *Nucl. Instrum. Methods Phys. Res. Sect. B Beam Interact. Mater. Atoms.* **441**, 108–118 (2019). <https://doi.org/10.1016/j.nimb.2017.01.043>
51. H. Silva, C. Santos, M. Fonseca, H. Luís, L. Martins, V. Manteigas, J. Cruz, A.P. Jesus, Measurement of gamma-ray production cross sections for nuclear reaction $31\text{P}(p, p\gamma)31\text{P}$. *Nucl. Instrum. Methods Phys. Res. Sect. B Beam Interact. Mater. Atoms.* **452**, 26–29 (2019). <https://doi.org/10.1016/j.nimb.2019.05.060>
52. IAEA Consultant's Meeting on Inter-comparison of PIGE Analysis Codes, 1–4 October 2018, IAEA, Vienna. (n.d.). <https://www-nds.iaea.org/index-meeting-crp/CM-PIGE-analysis2018/>. Accessed December 20, 2020
53. N. Pessoa Barradas, J. Cruz, M. Fonseca, A.P. de Jesus, A. Lagoyannis, V. Manteigas, M. Mayer, K. Preketes-Sigalas, P. Dimitriou, International atomic energy agency inter-comparison of particle induced gamma-ray emission codes for bulk samples. *Nucl. Instrum. Methods Phys. Res. Sect. B Beam Interact. Mater. Atoms.* **468**, 37–47 (2020). <https://doi.org/10.1016/j.nimb.2020.02.019>
54. C. Santos, Elemental analysis of bone samples affected by Osteoporosis and Paget's Disease of Bone, Faculdade de Ciências e Tecnologia (FCT), 2016. <https://run.unl.pt/handle/10362/20451>
55. M. Mayer, SIMNRA, a simulation program for the analysis of NRA, RBS and ERDA. *AIP Conf. Proc.* **475**, 541 (1999). <https://doi.org/10.1063/1.59188>
56. M. Mayer, Improved physics in SIMNRA 7. *Nucl. Instrum. Methods Phys. Res. Sect. B Beam Interact. Mater. Atoms.* **332**, 176–180 (2014). <https://doi.org/10.1016/j.nimb.2014.02.056>
57. I.A.E. Agency, Experimental Nuclear Reaction Data (EXFOR). (n.d.). <https://www-nds.iaea.org/exfor/exfor.htm>
58. I.A.E. Agency, Ion Beam Analysis Nuclear Data Library (IBANDL). (2020). <https://www-nds.iaea.org/exfor/ibandl.htm>
59. N.P. Barradas, N. Catarino, R. Mateus, S. Magalhães, E. Alves, Z. Siketić, I.B. Radović, Determination of the ${}^9\text{Be}(3\text{He}, \pi){}^{11}\text{B}$ ($i=0,1,2,3$) cross section at 135° in the energy range 1–2.5 MeV. *Nucl. Instrum. Methods Phys. Res. Sect. B Beam Interact. Mater. Atoms.* **346**, 21–25 (2015). <https://doi.org/10.1016/j.nimb.2015.01.037>
60. N. Catarino, N.P. Barradas, E. Alves, Determination of ${}^9\text{Be}(p, p_0){}^9\text{Be}$, ${}^9\text{Be}(p, d_0){}^8\text{Be}$ and ${}^9\text{Be}(p, \alpha_0){}^6\text{Li}$ cross sections at 150° in the energy range 0.5–2.35 MeV. *Nucl. Instrum. Methods Phys. Res. Sect. B Beam Interact. Mater. Atoms.* **371**, 50–53 (2016). <https://doi.org/10.1016/j.nimb.2015.10.062>